PROCEEDINGS OF THE INTERNATIONAL WORKSHOP ON

Mechanical Behavior *of* Thick Composites

Edited by:

SUONG V. HOA, Ph.D.

Workshop Chair, Concordia Center for Composites
Department of Mechanical and Industrial Engineering
Concordia University, Montreal, Quebec Canada

March 14–15, 2016
Montreal, Quebec, Canada

Sponsors:
Concordia University
Bell Helicopter
AHS Montreal Ottawa
CRIAQ
Concordia Centre for Composites
Indian Institute of Science (IISc)

Organizing Committee:
Suong Van Hoa, Workshop Chair, Concordia University, Canada
Rajamohan Ganesan, Concordia University, Canada
Dinesh Harursampath, Indian Institute of Science (IISc), India
Elliott Schulte, Bell Helicopter Textron Ltd., USA
James Corrigan, Bell Helicopter Textron Ltd., Canada
Francois Landry, Bell Helicopter Textron Ltd., Canada

DES*tech* Publications, Inc.

Mechanical Behavior of Thick Composites

DEStech Publications, Inc.
439 North Duke Street
Lancaster, Pennsylvania 17602 U.S.A.

Printed in the United States of America
10 9 8 7 6 5 4 3 2 1

Main entry under title:
Proceedings of the International Workshop on Mechanical Behavior of Thick Composites

A DEStech Publications book
Bibliography: p.
Includes index p. 139

ISBN No. 978-1-60595-319-9

Temperature Measurement in Autoclave Manufacturing Process for Thick Glass/epoxy Composite Laminate

Sara Mamani and Suong V. Hoa
Concordia Center for Composites
Department of Mechanical and Industrial Engineering
Concordia University
Montreal, Quebec, Canada
Center for Research in Polymers and Composites (CREPEC)
hoasuon@alcor.concordia.ca

Abstract

The temperature field in thick thermosetting composite laminate has a significant effect on the residual stresses during the curing process. In this study the temperature distribution of 18.28 mm glass/epoxy composite laminate manufactured by autoclave vacuum bag process were measured. The finite difference formulation of the one-dimensional transient heat transfer problems including internal heat generation was developed to simulate the heat transfer inside the autoclave to the laminated composite. The boundary condition of the laminate part was simulated entirely to consider the asymmetric condition in vacuum bag process. The calculated temperature profile was compared with the experimental result and it was found that the measured temperatures through the thickness agreed well with the numerical values. The overshoot in internal layers led to the temperature and cure gradient which has to be considered for the stress distribution and the final quality of the thick part.

Keywords: *Thermal field, Transient finite difference analysis, Thick thermoset composite laminate*

1 Introduction

The relevance of polymer composites, especially thick plate laminates to aerospace have increased to the point that they are used in the primary structures of aircrafts and have found several applications. Residual stress is the direct consequence of complex gradients of temperature and degree of cure and can have a significant effect on the mechanical performance of composite structures. Therefore, it is important to examine temperature distribution inside the part during the cure process. One of the concerns relates to high internal temperature due to the exothermic chemical reactions. Since the thermal conductivity of composites are low, the liberated heat during the irreversible chemical reaction cannot dissipate easily by conduction heat transfer mechanism, it raises internal part temperature leading to complex temperature and degree of cure gradients that develop during the curing process. Non-uniform curing is induced

owe to these gradients within the part may also result in spatial response of mechanical properties through the thickness which consequently lead to the process-induced stresses in the laminate plate.
In this paper, the temperature distribution is obtained based on the transient one-dimensional finite difference heat transfer formulation which is coupled to the cure kinetics of the thermoset composite materials. Moreover, the temperature profiles for thick glass/epoxy laminate are predicted and compared with experimental results. It is found that the numerical results have an acceptable agreement with experimental ones.

2 Thermo-Chemical Model

To investigate the temperature distribution and degree of cure during the composite manufacturing, a one dimensional cure simulation analysis was developed. It is assumed that the convective heat transfer effect due to resin flow is ignorable and fiber and resin are in thermal equilibrium condition at any specific time. Hence, the principal governing equation which is used to analyze the one-dimension heat transfer in the model is expressed as the following equation:

$$\rho_c C_{c,p} \frac{\partial T}{\partial t} = \frac{\partial}{\partial z}\left(k_{c,t} \frac{\partial T}{\partial z}\right) + q^{\cdot} \tag{1}$$

Here, the parameters T, $k_{c,t}$, ρ_c and $C_{c,p}$ are temperature, the through the thickness thermal conductivity, density and specific heat of the composite, respectively. In this study, these parameters are assumed to be constant during the curing simulation. In Equation (1), the term $q^{\cdot}$ is the internal heat generation, representing the transient heat liberated per unit volume of material from exothermic chemical reaction due to the cross-link polymerization.

$$q^{\cdot} = \rho_c H_u \frac{d\alpha}{dt} \tag{2}$$

Where H_u and $\frac{d\alpha}{dt}$ are the total liberated heat for the complete cure and the rate of cure, respectively. The rate of reaction, $\frac{d\alpha}{dt}$, is a function of degree of cure and temperature. It is required to compute the generated heat and degree of cure during the curing process [1]. The kinetic model utilized in this work is given by [2],

$$\frac{\mathrm{d}\alpha}{\mathrm{dt}} = \mathrm{g}(\alpha, \mathrm{T}) = (\mathrm{K}_1 + \mathrm{K}_2\alpha^{\mathrm{m}})(1-\alpha)^{\mathrm{n}} \tag{3}$$

$$K_i(T) = A_i exp\left(-\frac{E_i}{RT}\right) \qquad i = 1,2 \tag{4}$$

Here, m and n are the reaction orders. The kinetic parameters for glass/epoxy including the pre-exponential coefficients, A_1 and A_2, the activation energies, E_1 and E_2 , universal gas constant, R, and the total heat of reaction, H_u are summarized in Table 1.

Table 1. Cure kinetic parameters for glass/epoxy [2].

Parameter	Dimension	Value
A_1	sec^{-1}	55599
A_2	sec^{-1}	72908
E_1	J/mol	58383
E_2	J/mol	51341
m	-	0.58
n	-	1.43
H_u	J/ kg	541467

The assumption of thermal equilibrium condition permits the rule of mixture to be valid for composite thermal properties including volumetric heat capacity ($\rho_c C_{c,p}$), density (ρ_c) and longitudinal thermal conductivity. The volumetric heat capacity of the composite is expressed according to the Equation (5). However, the transverse conductivity is computed using Springer-Tsai model according to the following equations [2]:

$$\rho_c C_{c,p} = \vartheta_m \rho_m C_{p,m} + (1 - \vartheta_m)\rho_f C_{p,f} \tag{5}$$

$$\frac{k_{ct}}{k_m} = \left(1 - 2\sqrt{\frac{\vartheta_f}{\pi}}\right) + \frac{1}{B}\left[\pi - \frac{4}{\sqrt{1 - \left({B^2\vartheta_f}/{\pi}\right)}}\right] tan^{-1} \frac{\sqrt{1 - \left({B^2\vartheta_f}/{\pi}\right)}}{1 + B\sqrt{{\vartheta_f}/{\pi}}}, \tag{6}$$

$$B = 2\left(\frac{k_m}{k_f} - 1\right)$$

f and m subscripts are used to express the fiber and matrix in the equations (5) and (6) . A summary of computed thermal properties of glass/epoxy composite are presented in Table 2.

Table 2. Thermal-physical properties of E773/S2glass [2].

Material	Volume fraction (%)	Thermal conductivity k (W/$m.K$)	Specific Heat C_p (J/kg.K)	Thermal expansion coefficient (10^{-6}/ºC)	Density (gr/cm^3)
S2-glass	53	0.218	737	16	2460
Epoxy	47	1.04	1238	60	1280
Glass/Epoxy		k_{ct} = 0.385	871.545	α_1=1.75 e-5 α_2=5.998e-5	1915.8

3 One –dimensional Finite Difference Method for Temperature Field- Explicit Method

In typical lay-up of autoclaved-cured composite, the stacked prepreg is placed on the tool plate covered by the release film, caul plate and bleeder. The assembly is bagged with a standard nylon bagging. The scheme of boundary condition is shown in Figure 1. Thus, during the one-dimensional transient finite difference modeling, not only the laminate, but the tool, caul plate, release film, bleeder and vacuum bag are also included to examine the influence of tooling and bagging assembly on the temperature and degree of cure profiles. The effective thermal conductivity across the thickness of the release film, bleeder and vacuum bag are calculated from the thermal conductivity and thickness of individual components as shown in Equation (7) [3].

$$k_z^{eff} = \frac{h_{bg} + h_{fl} + h_{bd}}{\frac{h_{bd}}{k_{bd,z}} + \frac{h_{bg}}{k_{bg,z}} + \frac{h_{fl}}{k_{fl,z}}} \tag{7}$$

Where h_{bg} ,h_{bd} , h_{fl} , $k_{bg,z}$, $k_{bd,z}$ and $k_{fl,z}$ are the thickness and thermal conductivity of the vacuum bag, bleeder and release film through the thickness. It is worth mentioning that since there is a significant difference between the conductivity of the caul plate and the upper boundary material including release film, bleeder and vacuum bag, they are considered separately. The release film placed under the caul plate and on top of the peel ply is also modeled exclusively because of its location and small conductivity compared to caul plate. According to Equation (8), the equivalent density for the vacuum bag, bleeder and release film through the thickness are estimated.

$$\rho_{eq} = \frac{\sum m_i}{\sum V_i} = \frac{A\sum(\rho_i h_i)}{A\sum h_i} = \frac{\rho_{bg}h_{bg} + \rho_{fl}h_{fl} + \rho_{bd}h_{bd}}{h_{bg} + h_{fl} + h_{bd}} \tag{8}$$

Here, ρ_i and h_i are represented the density and thickness of each material. The heat balance formulations for each node are expressed according to Equation (9) to (12). The nodes extend from the top air-exposed surface, to the bottom surface of the plate.

$$hA\left(T_\infty{}^i - T_i{}^i\right) + k_z^{eff} A \frac{\partial T_j^i - \partial T_{j-1}^i}{\partial h_t} = \rho_{eq} C_{Av,p}\left(\frac{h_t}{2}A\right)\frac{\partial T_j^{i+1} - \partial T_j^i}{\partial t} \tag{9}$$

Here, h_t is the total thickness of the vacuum bag, bleeder and release film. Since the specific capacities of these materials are close to each other, the average value is selected.

$$k_{cl}A\frac{\partial T_{j-1}^i - \partial T_j^i}{\partial h_{cl}} + k_z^{eff}A\frac{\partial T_{j+1}^i - \partial T_j^i}{\partial h_t} = \left(\rho_{eq}C_{Av,p}\left(\frac{h_t}{2}A\right) + \rho_{cl}C_{cl,p}\left(\frac{h_{cl}}{2}A\right)\right)\frac{\partial T_j^{i+1} - \partial T_j^i}{\partial t} \tag{10}$$

In this equation h_{cl} , ρ_{cl} and $C_{cl,p}$ are the thickness, density and specific heat of the caul plate.

$$k_{fl}A\frac{\partial T_{j-1}^i - \partial T_j^i}{\partial h_{fl}} + k_{cl}A\frac{\partial T_{j+1}^i - \partial T_j^i}{\partial h_{cl}} = \left(\rho_{cl}C_{cl,p}\left(\frac{h_{cl}}{2}A\right) + \rho_{fl}C_{fl,p}\left(\frac{h_{fl}}{2}A\right)\right)\frac{\partial T_j^{i+1} - \partial T_j^i}{\partial t} \tag{11}$$

In this equation h_{fl} , ρ_{fl} and $C_{fl,p}$ are the thickness, density and specific heat of the release film.

$$k_{c,t}A\frac{\partial T_{j-1}^{i}-\partial T_{j}^{i}}{\partial z}+k_{fl}A\frac{\partial T_{j+1}^{i}-\partial T_{j}^{i}}{\partial h_{fl}}+\rho_{c}H_{u}(\frac{\Delta z}{2}A)\left(\frac{d\alpha}{dt}\right)_{j}^{i}=(\rho_{fl}C_{fl,p}(\frac{h_{fl}}{2}A)+\rho_{c}C_{c,p}(\frac{\Delta z}{2}A))\frac{\partial T_{j}^{i+1}-\partial T_{j}^{i}}{\partial t} \quad (12)$$

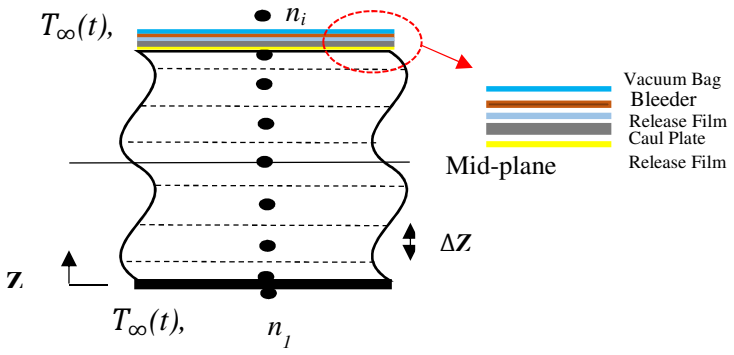

Figure 1. Schematic diagram of the asymmetric boundary condition.

4 Experiment

Experiments were conducted to verify the validity of the simulation and consider the effectiveness of the recommend cure cycle, using unidirectional glass/epoxy prepreg. The glass/epoxy prepreg used in this work was E773/S-2 Glass. The laminated plate was built up of the stacked plies with $4(in) \times 6(in) \times 0.72\ (in)$ dimension. When the stacked prepreg was placed on the tool plate with the thickness of 50 mm, it was covered by the release film. Afterwards, the caul plate was situated and the sample was surrounded by the dams in four edges, covered with the bleeder. The assembly was bagged with a standard nylon bagging according to Figure 2. The individual material properties are shown in Table 3. The convective heat transfer coefficient is 70 W/m^2 and the thermal contact resistance was assumed to be negligible. The recommended cure cycle in Figure 6 includes two stages; first, consolidation and then full cure. The former begins with temperature raise from room temperature to 170 ºF with the rate of 2 ºF/min and then the temperature is kept constant for about 60 minutes. Resin bleeding occurs during the first stage. While in the latter stage, the temperature rises with the same heat rate as the former stage. As soon as the temperature reaches 275 ºF, the resin cure temperature, the temperature is maintained for 60 minutes. In this way, the full cure of the sample is achieved.

Table 3. Thermal-physical properties of the bagging process material [4].

Material	Thermal Conductivity (W/m K)	Specific Heat (J/g K)	Density (g/cm^3)
Aluminum	220	0.903	2.72
Release film	0.5	1.04	2.2
Bleeder	0.07	1.35	0.26
Bag	0.24	1.67	1.14

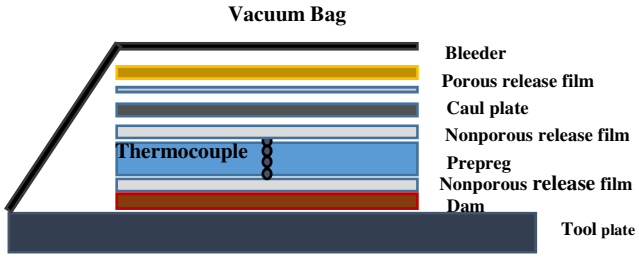

Figure 2. The typical composite lay-up cured in the autoclave.

As can be seen in Figure 2, in order to examine the variation of temperature inside the laminate during the curing process, total of five thermocouples were located in the laminate: over the plate/under the center point of the bottom layer, at center of the laminate, and at the top surface of the laminate.

5 Results and Discussion

Due to the low thermal conductivity and large thickness of glass/epoxy composites, usually a significant amount of temperature lag and overshoot at the center of laminates is experienced during the cure cycle. In this study, the temperature profile of 18.28 mm thick glass/epoxy laminate during an autoclave vacuum bag process was assessed from numerical simulation and experiment. According to temperature measurements through thermocouples, the temperature profile for unidirectional laminate is presented in Figure 3. A temperature overshoot is observed from the experimental results. It can be seen from Figure 3, the temperature overshoot related to the mid-point of the center section is 305 ºF, and the maximum temperature difference between the center section and upper and lower edges is respectively 15 and 50 degree after 195 min during the curing process. Accordingly, this cause severe temperature gradient and non-uniform curing inside the part.

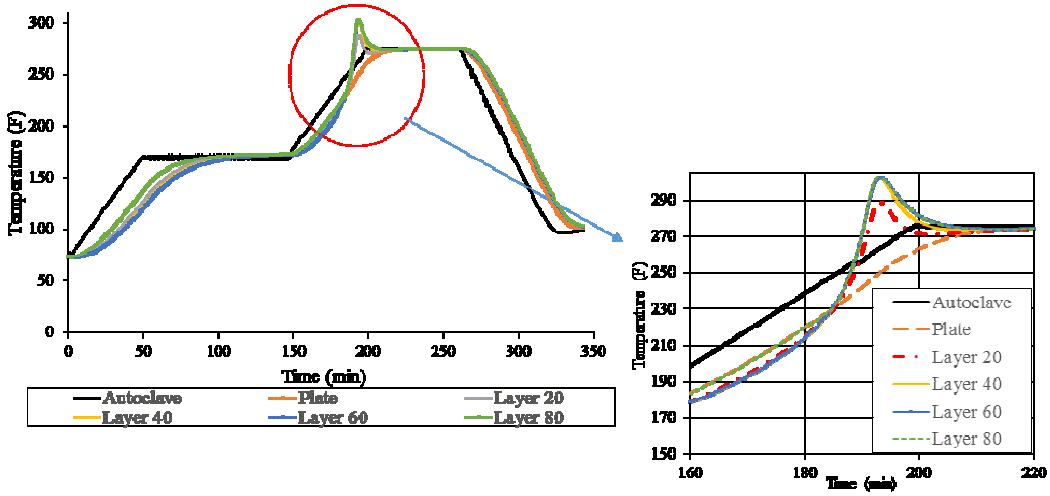

Figure 3. Temperature profile in unidirectional glass/epoxy laminate from experiment.

In Figure 4, the temperature distributions at different time during the cure cycle are illustrated for unidirectional laminate. At beginning, the maximum temperature happens on the outside and the

Failure Analysis of Thick Composite Beams: A Comparative Study of Various Failure Theories

Satish Garella, Umesh Kizhakkinan and Dineshkumar Harursampath
NMCAD Lab
Department of Aerospace Engineering
Indian Institute of Science
Bengaluru, India

ABSTRACT

Thick composite beams are used as primary structural members in various engineering applications, for example, composite flex beams in a hinge less rotor system of modern helicopters. One end of the flex beam yoke is connected to the rotor hub through joints and the other end is connected similarly to the rotor blade. A flex beam yoke has to support rotating loads, vibratory bending loads and torsional loads. It should be strong enough to hold the blade yet flexible enough to allow for the flapping motion. Hence, it is essential to understand the mechanism of stress development, crack initiation and propagation in a bolted thick composite beam, which is subjected to axial and flexural loads.

A unidirectional glass/epoxy thick composite beam is considered in this study. A common engineering practice is to use bolted joints to attach two structural members and the bolts are pre-tensed. Buffer pads are attached to the composite beam to avoid localized damage. To simulate the real life situation, a CAD model is generated using ABAQUS [1] consisting of a thick composite beam with eight bolt holes, buffer pads, steel clamping blocks, steel washers and steel bolts. The composite beam is attached to a rigid block using a clamping block, washers and bolts. The finite element mesh is generated using 3-D continuum elements, C3D8I. Nonlinear stress analysis is performed for bolt pre-tension and bending loads with material and contact nonlinearity. The numerical results depend on the element type in finite element analysis. Parametric study for element selection between SC8, C3D8 and C3D20 is carried out. The finite element analysis results are compared with the experimental values.

Different failure criteria are considered to study the failure behavior of the thick composite beam: Tsai-Wu, Christensen, and Puck, Hashin and quadratic delamination failure criteria.

These failure criteria are coded in ABAQUS through user subroutines. The bolt holes act as stress concentration regions in the beam, where the failure behavior is studied utilizing the above criteria. The effect of different loading, such as bolt pre-tension, bending on the failure of the composite thick beam are investigated.

MODELING

Dimensions for components like flex beam, bolts, washer and rigid fixed support are used from the Figure.1 modelled in ABAQUS. All the dimensions are converted to millimeters in the model.

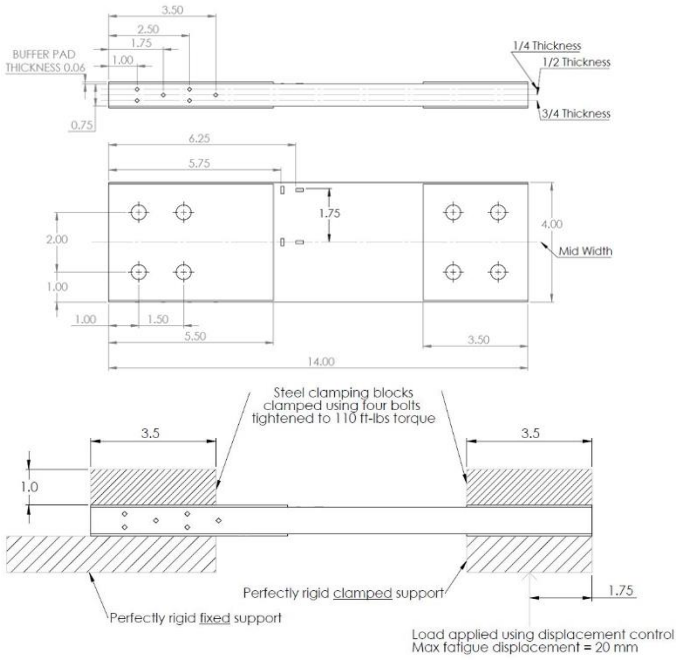

Figure.1: Dimensions, Load and Clamped Area

Material Properties

Flex beam specimen is assigned with material data shown in Table 1. Bolts, Washers and Steel Clamping blocks are assigned with **Steel (UNS30400) Alloy [3]** Material properties shown in Table 2. Buffer pads are assigned glass material properties taken from literature survey. To perform the elastic-plastic analysis, the elastic mechanical properties are still required because this will provide the stress-strain relationship up to the yield point but additional information is required to ensure the plastic range is accurately developed. To develop the plastic range in FEA, the yield stress and plastic strain need to be manually loaded into the material properties.

TABLE I. FLEX-BEAM MATERIAL PROPERTIES

Flex beam Material Properties	
E_{11} (GPa)	49.9
E_{22} (GPa)	7.9
E_{33} (GPa)	7.9
G_{12} (GPa)	4.9
G_{13} (GPa)	4.9
G_{23} (GPa)	3.8
ν_{12}	0.3
ν_{13}	0.3
ν_{23}	0.4

TABLE II. OTHER COMPONENTS

Clamping block (Steel)	
E(GPa)	188
ν	0.3
Bolt (Steel)	
E(GPa)	188
ν	0.3
Washer (Steel)	
E(GPa)	188
ν	0.3
Buffer pad (Glass)	
E(GPa)	70
ν	0.23

The Equation (1) below is used to generate Stress Strain Curve. Figure.3 shows Stress Strain curve from Yield Stress (612Mpa) to Ultimate Stress (782Mpa).

$$\varepsilon = \frac{\sigma-\sigma_{0.2}}{E_{0.2}} + \varepsilon_u * \frac{\sigma-\sigma_{0.2}}{\sigma_u-\sigma_{0.2}}^{3.746} + \varepsilon_{0.2} \quad \text{For} \quad \sigma > \sigma_{0.2} \qquad \ldots (1)$$

To perform this analysis 39 yield stresses and plastic strains points were manually loaded into the plastic material properties module. Note that the fully elastic material properties are also present in the material properties to ensure that stress applied up to the yield point is elastic. The way ABAQUS analyzes an elastic-plastic problem is by using the fully elastic material properties until the yield point is achieved and then it starts to apply the plastic material properties. Table III shows strength properties where tensile and compressive allowable strengths for lamina are denoted by subscripts *T* and *C*, respectively. X_T, Y_T, Z_T denotes the allowable tensile strengths in three respective material directions. Similarly, X_C, Y_C, Z_C denotes the allowable tensile strengths in three respective material directions. Further, S_{12}, S_{13} and S_{23} denote allowable shear strengths in the respective principal material directions.

TABLE III. GLASS/EPOXY FAILURE MATERIAL PROPERTIES

Longitudinal Tensile Strength X_T (GPa)	1000
Longitudinal Compressive Strength X_C (GPa)	600
Transverse Tensile Strength Y_T (GPa)	30
Transverse Compressive Strength Y_C (GPa)	120
Longitudinal Shear Strength S_{12} (GPa)	70
Transverse Shear Strength S_{13} (GPa)	70

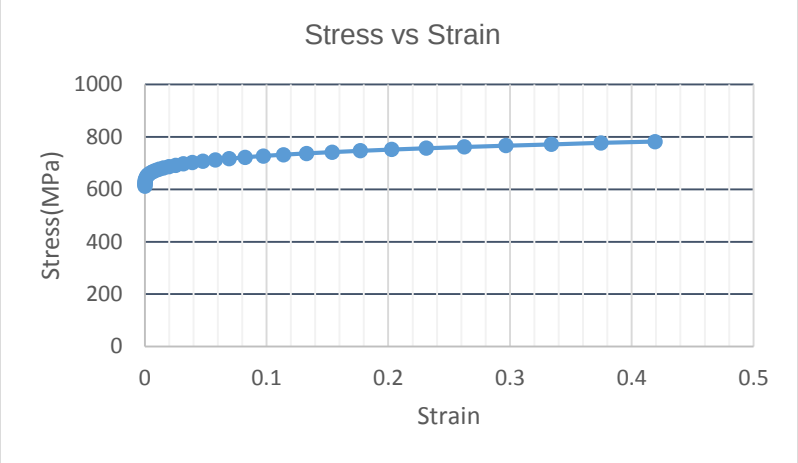

Figure.3: Stress Strain Curve for **Steel (UNS30400) Alloy.**

Element Selection

Unidirectional 80 plies are considered in the analysis. Through thickness 8 elements are used. Each element takes 10 plies. For all other Components like Bolts, Washers, Steel clamping blocks and Buffer pads Continuum three dimensional 8 noded Incompatible (**C3D8I)** element is used. Rigid fixtures are modelled with Rigid three dimensional 4 noded (**R3D4)** and Rigid three dimensional 3 noded (**R3D3)** elements. The modes of failure that examined are delamination, matrix compression failure, fiber compression failure, matrix tensile failure and fiber tensile failure, interlaminar tensile failure and interlaminar matrix failure. Hashin [2], Puck [3], Christensen [3], Tsai-Wu [4], Quadratic delamination [5] and Hoffman failure [4] criterion are coded in subroutine for finding the critical regions of failure and mode of failures

BOUNDARY CONDITIONS AND LOADING

Flex beam buffer pads and steel clamping blocks are modelled as single component. It means there is node to node connectivity between all these components. This is done mainly to avoid contacts between flex Beam and buffer pads. Tie constraints are applied between steel block and washers, washers and bolts, and, buffer pads and rigid fixtures. Surface to surface contacts are applied between bolt hole surface, steel block, washer, buffer pads, flex-beam and rigid fixtures as shown in Table IV. Bolts are grounded using weak springs (stiffness is2N) to avoid rigid body mode. Strain free adjustment of nodes is allowed after pretension loading to avoid Contact Convergence issues. Two load steps are considered during this analysis. First loading step is pretension and second loading step is bending.

TABLE IV. CONTACT DETAILS FOR VARIOUS COMPONENTS

	Bolts	**Washers**	**Steel Plate**	**Buffer Pad**	**Flex beam**	**Rigid Stand**
Bolt		Bonded (Tie)	Standard	Standard	Standard	Standard
Washer	Bonded (Tie)		Standard			
Steel Plate				Standard		
Buffer Pad			Standard		Bonded (Tie)	
Flex Beam				Standard		
Rigid Stand					Standard	

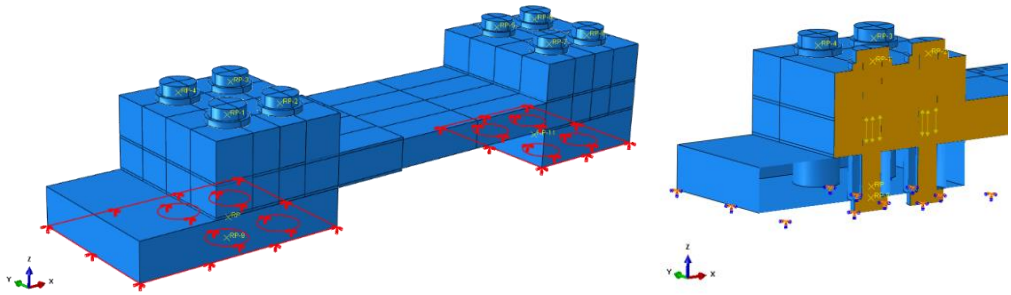

Figure.7: Pretension boundary condition and loading details.

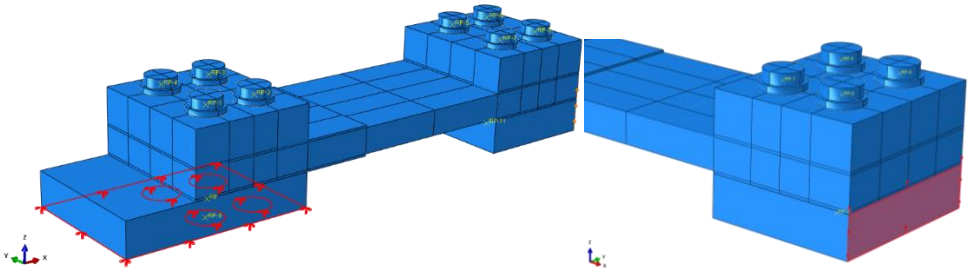

Figure.8: Bending load boundary condition and loading details

Pretension load of 60.4KN as shown in Figure.7. Bending displacement of 40mm is applied at loading end of rigid fixture. Red lines in the Figure.7 and Figure.8 indicate

Author Index